

Landslides (2011) 8:67–79
 DOI 10.1007/s10346-010-0228-6
 Received: 24 July 2009
 Accepted: 21 May 2010
 Published online: 16 July 2010
 © Springer-Verlag 2010

Giovanna Capparelli · Pasquale Versace

FLaIR and SUSHI: two mathematical models for early warning of landslides induced by rainfall

Abstract The development of Early Warning Systems in recent years has assumed an increasingly important role in landslide risk mitigation. In this context, the main topic is the relationship between rainfall and the incidence of landslides. In this paper, we focus our attention on the analysis of mathematical models capable of simulating triggering conditions. These fall into two broad categories: hydrological models and complete models. Generally, hydrological models comprise simple empirical relationships linking antecedent precipitation to the time that the landslide occurs; the latter consist of more complex expressions that take several components into account, including specific site conditions, mechanical, hydraulic and physical soil properties, local seepage conditions, and the contribution of these to soil strength. In a review of the most important models proposed in the technical and international literature, we have outlined their most meaningful and salient aspects. In particular, the Forecasting of Landslides Induced by Rainfall (FLaIR) and the Saturated Unsaturated Simulation for Hillslope Instability (SUSHI) models, developed by the authors, are discussed. FLaIR is a hydrological model based on the identification of a mobility function dependent on landslide characteristics and antecedent rainfall, correlated to the probability of a slide occurring. SUSHI is a complete model for describing hydraulic phenomena at slope scale, incorporating Darcian saturated flow, with particular emphasis on spatial-temporal changes in subsoil pore pressure. It comprises a hydraulic module for analysing the circulation of water from rainfall infiltration in saturated and nonsaturated layers in non-stationary conditions and a geotechnical slope stability module based on Limit Equilibrium Methods. The paper also includes some examples of these models' applications in the framework of early warning systems in Italy.

Keywords Landslide · Mathematical models · Rainfall

Introduction

Early warning systems for reducing the risks associated with landslides play a significant and increasing role in several countries (IFLDM 2007; ILF 2008; IWL 2009). The technical literature contains many examples of systems developed in recent years. These include the Landslip Warning System used in Hong Kong since 1977, continually updated and improved over the years (Pun et al. 2003; Yu et al. 2004); the system developed in California to prevent the consequences of rainfall-induced debris flows in the San Francisco Bay area (Keefer et al. 1987), and in Nagasaki (Yano and Senoo 1985); the Rio-Watch system set up for Rio de Janeiro (D'Orsi et al. 1997); and in many other places, including New Zealand (Glade et al. 2000), the UK (Cole and Davis 2002), Italy (Versace and Capparelli 2008), Washington (Baum et al. 2005), and Indonesia (Fathani et al. 2009; Takara and Apip Bagawan 2009).

Early warning systems mitigate risk by giving sufficient lead time to implement actions to protect persons and/or property.

Risk mitigation is not only limited to physical measures but also includes research into ways of improving methods of assessment and quantification of landslide occurrence and producing guidelines for choosing the most appropriate risk management strategies (Kalsnes et al. 2009). An early warning system, therefore, requires a chain of functional components: landslide susceptibility maps for the investigated areas; scenarios for event impact on exposed people and goods; monitoring of key parameters and real-time data transmission; mathematical modeling and data processing for both current hazard evaluation and future hazard forecasting; warning models; emergency plans in order to avoid or reduce damage and injury or loss of life; and decision-making procedures.

From a general point of view, there are four characteristic times in landslide early warning (Fig. 1):

- t_1 *evolution delay*—the time between the landslide onset and its impact
- t_2 *lag*—the time between precursor occurrence and landslide triggering
- t_3 *nowcasting delay*—the time between forecasting and occurrence of the precursor
- t^* *intervention delay*—the time necessary both for making decisions and initiating action such as evacuation and protection of structures and infrastructure.

Rainfall is largely adopted as a precursor in early warning of landslides, owing to the large prevalence of landslides induced by precipitation. When $t^* < t_1$, monitoring of movement may be enough. When $t_1 < t^* < (t_1 + t_2)$, also amount of rainfall must be measured.

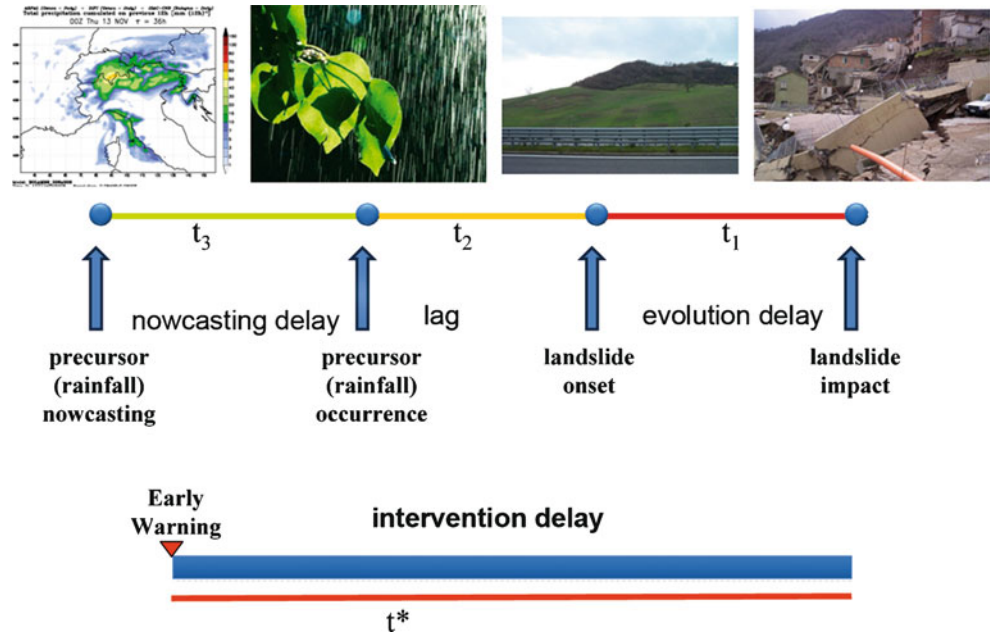
Finally, when $t^* > (t_1 + t_2)$, rainfall nowcasting becomes essential. The relationship between landslide triggering and antecedent rainfall is the most important issue in landslide forecasting and has been widely investigated. There are many modelling approaches to be found in the literature that use back-analyses of data from observed landslides to determine the relationships between precipitation and landslide occurrence.

The models differ greatly according to the geological context and the involved processes of rainfall influence on slope stability. In addition, differences in the models depend on:

- the level of detail used to describe the hydrological and geotechnical processes in the slope being analyzed;
- the spatial scale, ranging from large areas up to ten of thousands of square kilometers, to small areas encompassing a single landslide;
- the quality and quantity of available hydrological, hydraulic, and geotechnical data.

Prediction of rainfall-induced landslides is mostly carried out using so-called *hydrological* (or *empirical* models (Cascini and Versace 1988)) that are based on historical data for

Fig. 1 Representation of four characteristic times in landslide early warning systems



landslides and related antecedent rainfall and do not require field instrumentation or measurements (Campbell 1975; Caine 1980; UNDRO 1991; Wilson and Wiczorek 1995; Sirangelo and Versace 1996).

Empirical approaches differ as to the duration of antecedent rainfall that needs to be taken into account, depending on the surface characteristics at the location being investigated, and on the area and depth of the landslide. For shallow landslides—soil slips, debris flows etc.—it is usually sufficient to consider only the precipitation within an antecedent interval of a few hours, the precise duration depending on the hydraulic conductivity of the soil. For landslides of greater size, however, it may be necessary to consider time horizons up to many months in duration.

As to size, the area affected by the phenomenon can range from a local scale where the analysis of a single hillslope or even an individual slide is required, up to a regional scale—a much more extended area up to several tens of thousands of square kilometers. The extent of the investigation area obviously conditions the need for sufficiently homogeneous geological, geomorphological, and land-use conditions. Homogeneity represents a particularly strict requirement, especially at hillslope scale.

The limitations of empirical models are typical of empirical methods in general in that they adopt simplifying assumptions about very complex phenomena by combining an extraordinarily large range of information. Furthermore, the use of a threshold function introduces excessive approximations.

Another relevant limitation is the use of cumulative rainfall data or rainfall of average intensity, in the mobilization function, neglecting to distinguish between different patterns in rainfall events. In addition, the threshold function is almost always empirically fixed by a line separating events associated with and without landslides.

Hydrological models are distinct from *physically based* (or *complete*) models, whose purpose is to reproduce the physical behavior of the processes involved at hillslope scale. These models are complex and need many site investigations. Looking at the models proposed in the technical literature, it is possible to make a general distinction between regional and local (or *point*) models. The former develop analyses over a wide area, usually producing a susceptibility map characterizing the landslide-prone zones (Montgomery and Dietrich 1994; Rigon et al. 2006). Local models, by comparison, analyze situations confined to a single slope or a single movement, employing detailed hydrological, hydraulic, and geotechnical information (Iverson 2000; Tsai and Yang 2006; Capparelli et al. 2009a, b).

Following a general framework, the physically based models are composed of two coupled modules: a hydrological module, for describing the porewater pressure and water movement within porous materials in space and time, and a geotechnical module for analyzing the slope stability conditions.

The main differences between the various complete models are to do with their capacity to capture the surface topography and its effects on overland flow and surface runoff concentration, the description of infiltration phenomena, the methodologies used to simulate underground water flow, and the techniques adopted for slope stability evaluation.

In this paper, two models, called Forecasting of Landslides Induced by Rainfall (FLaIR) and Saturated Unsaturated Simulation for Hillslope Instability (SUSHI), are proposed.

The first one can be considered as a general framework of the empirical models, given that it includes, as special cases, the most commonly models used in technical literature: those based on intensity duration (I-D) thresholds (Guzzetti et al. 2007), and other empirical approaches such as those proposed by D'Orsi et al. (1997), Gabet et al. (2004), and Wilson and Wiczorek (1995).

The second one is a local complete model of which the paper introduces the main features and an application to a real case.

General description

In empirical models, it is possible to identify a mobility function $Y(t)$, which is a generic function of the antecedent rainfall that can be correlated with landslide occurrence. More precisely, if $P[E_t]$ is the probability of occurrence of a landslide at time t , and if we assume that $P[E_t]$ depends only on $Y(t)$, we can express $P[E_t]$ as:

$$P[E_t] = \begin{cases} 0 & \text{if } Y(t) < Y_1 \\ g[Y(t)] & \text{if } Y_1 \leq Y(t) \leq Y_2 \\ 1 & \text{if } Y(t) > Y_2 \end{cases} \quad (1)$$

where $g[\cdot]$ is a non-decreasing generic function that can take values between $[0;1]$ in the interval $[Y_1; Y_2]$; Y_1 is the value of $Y(t)$ for which mobilization is impossible; and Y_2 is the value of $Y(t)$ for which mobilization is certain.

By assuming that $Y_1=Y_2=Y_{cr}$, we identify a threshold value Y_{cr} of a mobility function $Y(t)$ which separates the condition “impossible mobilization” from “certain mobilization”; that is:

$$\begin{cases} P[E_t] = 0 & \text{if } Y(t) < Y_{cr} \\ P[E_t] = 1 & \text{if } Y(t) \geq Y_{cr} \end{cases} \quad (2)$$

The choice of criteria adopted by different authors for defining threshold values varies greatly: e.g., Cannon and Ellen (1985) assume that the threshold corresponds to “abundant landslides,” while for Wieczorek (1987), the threshold corresponds to “one or more than one landslides.” Nevertheless, the threshold approach remains the most widely used in rainfall–landslide studies, because of the difficulty in function identification and parameter calibration in Eq. 1 owing to the lack of experimental data.

Sirangelo and Versace (1992) proposed the hydrological model FLaIR, which considers the mobility function as a convolution between the rainfall intensity $I(\cdot)$ and a filter function $\psi(\cdot)$:

$$Y_F(t) = \int_0^t \psi(t - \tau)I(\tau)d\tau \quad (3)$$

where the F subscript denotes FLaIR.

The function $\psi(\cdot)$ is typical for each case study and plays a central role in mobility function evaluation. It can assume different expressions (Iiritano et al. 1998), such as:

$$\text{rectangular : } \psi(t) = \begin{cases} 1/t_0 & \text{if } 0 < t \leq t_0 \\ 0 & \text{elsewhere} \end{cases} \quad (4)$$

$$\text{exponential : } \psi(t) = \frac{1}{k} e^{-t/k} \quad t \geq 0, k > 0 \quad (5)$$

$$\text{gamma : } \psi(t) = \frac{b^a}{\Gamma(a)} t^{a-1} e^{-bt} \quad t \geq 0, a > 0, b > 0 \quad (6)$$

$$\text{power : } \psi(t) = mt^{-q} \quad 0 < t < T, m > 0, 0 < q < 1 \quad (7)$$

mixture of two exponential functions :

$$\psi(t) = \omega\beta_1 \exp(-\beta_1 t) + (1 - \omega)(-\beta_2 t) \quad t \geq 0, \beta_1 \geq \beta_2 > 0, 0 \leq \omega \leq 1 \quad (8)$$

Equation 8, in particular, is very flexible and allows for two different kinds of rainfall interaction: the first addendum reproduces the effect

of the most recent rainfall (short-term component); the second addendum reproduces the effects also of earlier rainfalls (long-term component). The terms ω and $(1-\omega)$ are the weights of the two components. Figure 2 shows the differences in mobility function when different filter functions are adopted to transform rainfall patterns.

FLaIR model acting as a general framework for rainfall–landslide empirical thresholds

Many empirical models can be considered as special cases of the FLaIR model. This is the case of the I–D models that are the most frequently used for analyzing shallow landslides on a regional scale. In this kind of model, the mobility function $Y_1(t)$ is given by the average rainfall intensity I over time intervals D , where $D \leq T$ hours, and the critical value, I_{cr} , of the mobility function depends on rainfall duration D . Therefore, the threshold is represented by a curve on the I–D (intensity–duration) plane. A power function relationship between I_{cr} and D is often considered:

$$I_{cr} = aD^{-b} \quad D \leq T \quad (9)$$

The value of T usually ranges between 24 and 100 h, but for deeper landslides, T may be larger up to tenth of days.

In other models (e.g., Corominas and Moya 1999), cumulative rainfall is assumed for the mobility function; adaptation to the I–D scheme is then straightforward. For comparisons between relationships for landslides in different climatic regions, a normalized rainfall intensity (rainfall intensity divided by average annual rainfall for the region) is usually considered. Guzzetti et al. (2007) have produced a broad review of the various formulas proposed for the I–D relationship.

If in Eq. 3, we assume the power filter function in Eq. 7, with parameters $q = 1 - b$ and $m = bT^b$, and where b and T are given by Eq. 9, and we also consider, as input, a rainfall event of duration D and a constant intensity I given by Eq. 9, we obtain:

(a) For $0 \leq t \leq D$:

$$\begin{aligned} Y_F(t) &= I \int_0^t \psi(t - \tau)d\tau = I \int_t^0 -\psi(u)du \\ &= aD^{-b} \int_0^t \frac{b}{T^b} u^{-(1-b)} du = \frac{a}{T^b} \left(\frac{t}{D}\right)^b \end{aligned} \quad (10a)$$

(b) For $D < t \leq T$:

$$\begin{aligned} Y_F(t) &= \int_0^D I\psi(t - \tau)d\tau + \int_D^t I\psi(t - \tau)d\tau = I \int_0^D \psi(t - \tau)d\tau \\ &= I \int_t^{(t-D)} -\psi(u)du = \frac{a}{T^b} \left[\left(\frac{t}{D}\right)^b - \left(\frac{t-D}{D}\right)^b \right] \end{aligned} \quad (10b)$$

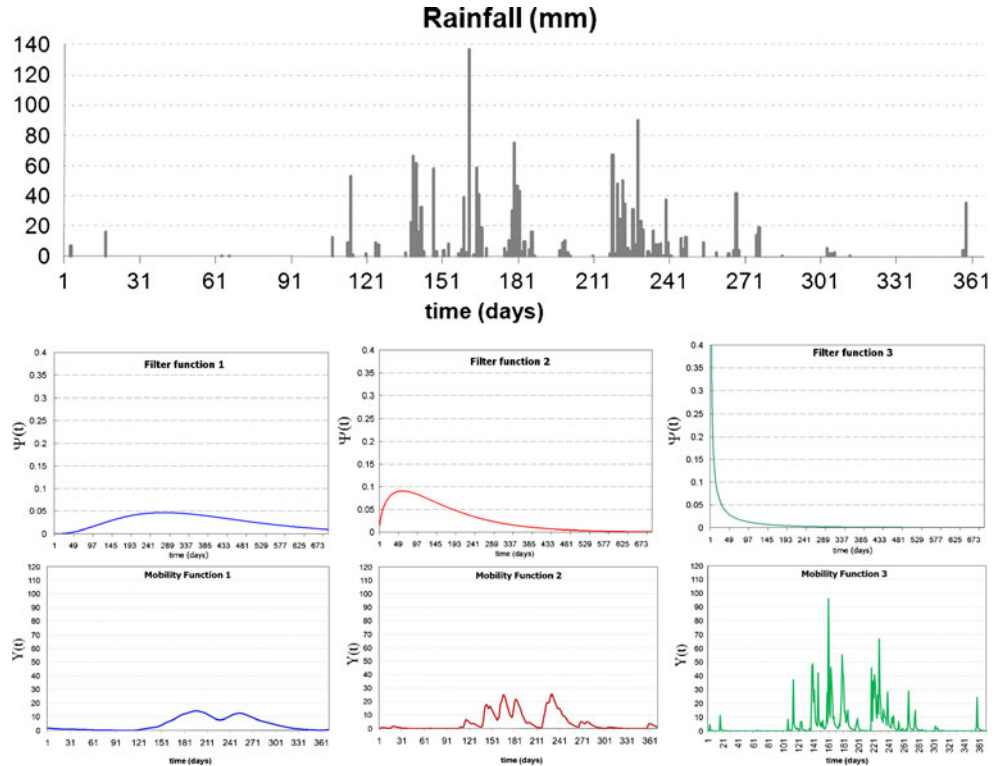
where $u = t - \tau$.

The maximum value of the mobility function is at $t=D$:

$$Y_{F,max} = \frac{a}{T^b} \quad (11)$$

The maximum value of the FLaIR mobility function given by Eq. 11 does not depend on duration D but only on the parameters in Eq. 9.

Fig. 2 Rainfall pattern; different adopted filter functions; obtained mobility functions



It represents the critical value for the mobility function $Y_F(t)$, since it corresponds to the critical relationship given by Eq. 9.

Thus, the FLaIR procedure involves assessing the mobility function by adopting the power filter function in Eq. 7 with $q = 1 - b$ and $m = b/T^b$ and a, b , and T given by Eq. 9, then comparing its current value with that given by Eq. 11. This is exactly equivalent to the procedure of comparing the current average rainfall intensities for different duration D ($D \leq T$ hours) with the critical values given by Eq. 9.

Consequently, all empirical models which follow Eq. 9 can be considered as special cases of the general relationship in Eq. 3; for example, the well-known Caine (1980) relationship (Fig. 3a):

$$I_{cr} = 14.82D^{-0.39} \quad 0 < D \leq 500 \quad (12)$$

can be represented by the FLaIR mobility function, with the following power filter function:

$$\psi(t) = 0.035t^{-0.61} \quad 0 < t \leq 500 \quad (13)$$

Figure 3b shows the pattern of $Y_F(t)$ derived from Eq. 12 for three different rainfall inputs with duration D and constant intensity I . In all cases, the maximum value of the mobility function is given by Eq. 11 and is equal to 1.32. So, applying the Caine approach, we can assume in the FLaIR model the critical value:

$$Y_{F,cr} = 1.32 \quad (14)$$

A second group of empirical models considers the mobility function $Y_R(t)$ to be the cumulative rainfall R_d during a fixed

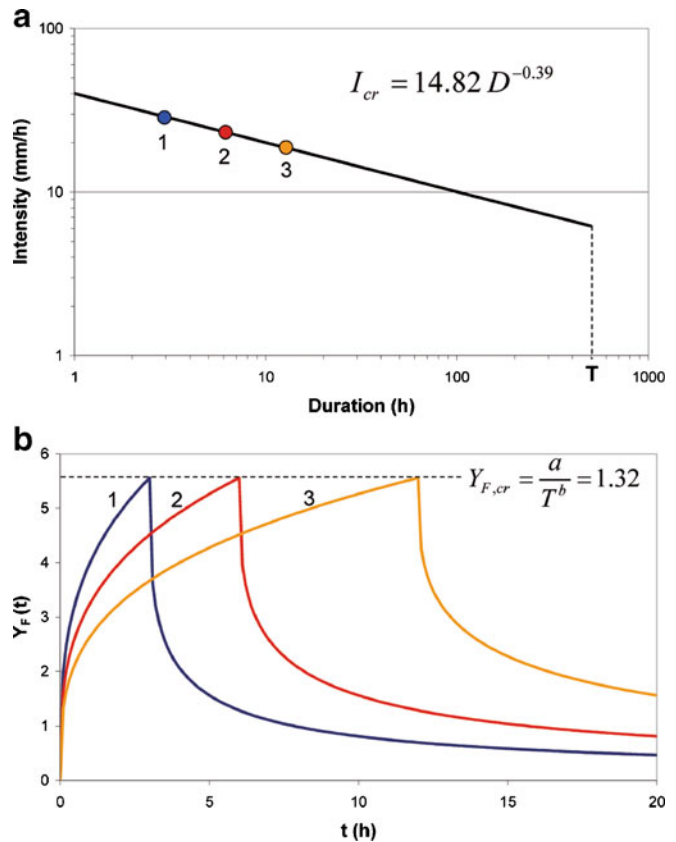


Fig. 3 a Caine I–D relationship with duration and related constant intensities adopted as inputs in FLaIR model; b FLaIR mobility functions for the selected inputs

period d , usually ranging from 1 h to a few days. The critical value of R_d is not constant but depends on antecedent rainfall aggregated over a duration $D > d$, namely R_D , which ranges from a few days to months, usually commencing at the beginning of the rain event, or at the beginning of the wet season. The intervals d and D may be disjoint or overlapped. Methods proposed by d’Orsi et al. (1997) and Gabet et al. (2004) can be considered as examples of this group. Also, in such cases, the FLAIR model can be adopted, in fact, assuming for $\psi(t)$ the rectangular (uniform) distribution in Eq. 4 in the interval $(0, d)$, it results in $Y_F(t) = Y_R(t)$. The method proposed by Wilson and Wiczorek (1995), based on the “leaky barrel” model, can also be considered as special case of Eq. 3, assuming for $\psi(\cdot)$ the exponential function of Eq. 5.

Thus, the FLAIR model can be regarded as a general framework for the majority of empirical relationships between landslides and antecedent rainfall. Moreover, the FLAIR model has many advantages compared with other empirical approaches. First, it is able to consider the real pattern of rainfall input, as it gives different values for the mobility function for rainfalls having the same average intensity but with different hyetographs (Fig. 4). Other models, such as I-D or R_d give, instead, a single value for the mobility function.

Comparison between current rainfall values and critical rainfall is more straightforward when using FLAIR because it compares just two values ($Y_F(t)$ and $Y_{F,cr}$) rather than two curves. In addition, depending on the shape of the filter function $\psi(\cdot)$, in the FLAIR model the weight attributed to a short and intense rainfall pulse

changes with time, whereas this cannot be accounted for if only cumulative rainfall is considered as in other empirical models. As a result, in the FLAIR model, the effect of such a rainfall pulse is not lasting. Finally, since the filter function $\psi(\cdot)$ can assume various shapes, the FLAIR model is much more flexible than other models and is able to represent different kinds of slope responses with respect to rainfall input, from very fast to slow responses.

Typical applications of the FLAIR model

Different applications can be carried out using FLAIR model. It is very flexible and can be used for different purposes. In this section, we draw attention to possible uses with information about some recently developed applications and provide references for further details.

The model can be used for single landslide applications analyzing historical cases of mobilization. Starting from the historical information—that is, landslide dates and antecedent rainfalls—it is possible to define the transfer function, the mobility function and threshold values (Eq. 2) (Sirangelo and Versace 1996; Iiritano et al. 1998). The many applications in several selected case studies in Italy have verified that the transfer function shapes appear to be accurately linked to landslide dimensions (Sirangelo et al. 2003). The triggering mechanisms for shallow landslides are usually very intense rainfall events of short duration; conversely, deep landslide movements can follow rainfall occurring over long periods of time. Typical function shapes obtained for these cases are shown in Fig. 5: curve (a), obtained for the Sarno mudflow (Sirangelo et al.

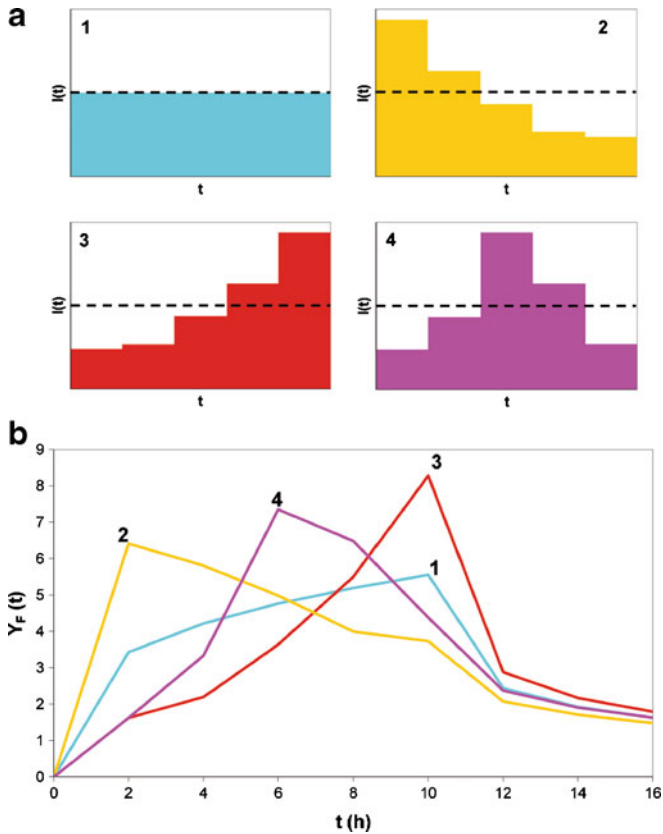


Fig. 4 a Hyetographs with the same duration and average intensity; b behavior of related mobility function

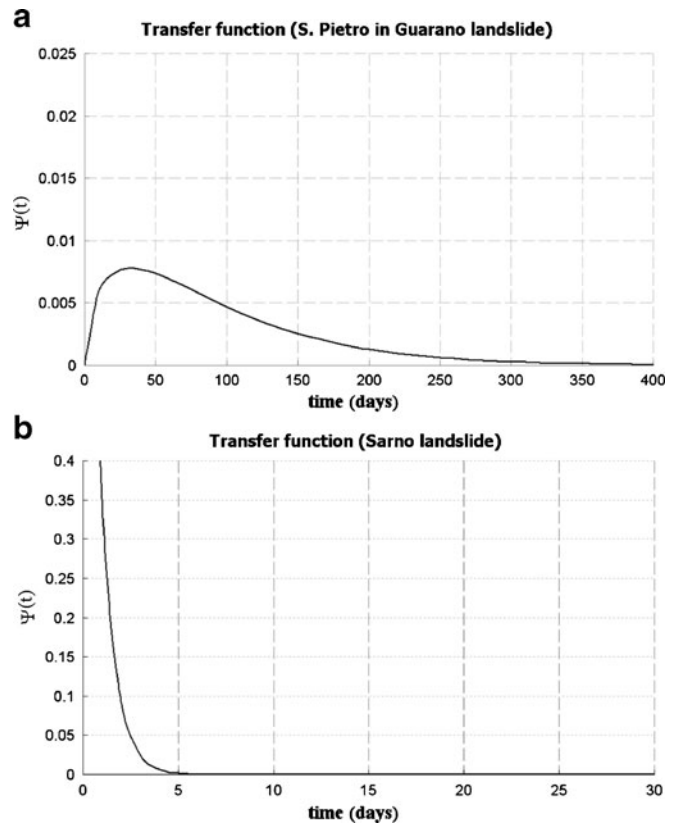


Fig. 5 Curve (a) Transfer function for landslide with short lag time from rainfall—two negative exponential functions (eq. 8) with $\omega=1$, $\beta_1=0.4 \text{ day}^{-1}$, $\beta_2=0.01 \text{ day}^{-1}$. Curve (b) Transfer function for landslide with long lag time from rainfall—gamma function (eq. 6) with $\alpha=1.4$, $b=2$ days

1998) highlights the effect of recent rainfall; curve (b) obtained for the San Pietro landslide (Cascini and Versace 1988) attributes more weight to the earlier rainfalls.

It is possible to link the FLAIR model to rain forecast models such as meteorological or stochastic generators which predict the probability of future rain events. These provide the input for the FLAIR model, which then evaluate the probability that the mobility function will exceed, at some future time t , the critical value, thus providing useful advance information about the evolving conditions. Capparelli and Tiranti (2010) describe an example concerning phenomena occurring in the Western Alpine sector of the Piemonte region (Northern Italy) where slope debris flows are the predominant landslide type. By linking the mobility function to meteorological forecasts, the model was used in the development of the MoniFLAIR early warning system for real-time monitoring and forecasting of slope hazards. Versace et al. (2007) and Giorgio et al. (2009) describe cases of the integration of FLAIR with different stochastic modules: Prediction of Rainfall Amount Inside Storm Events proposed by Sirangelo et al. (2007) and Disaggregated Rectangular Intensity Pulse proposed by Heneker et al. (2001). In all these cases, the outputs are represented as the probability, estimated at time τ , that the forecast value of the mobility function $Y_r(t)$ will exceed the critical value at time $t > \tau$.

If suitable, geotechnical monitoring instrumentation (inclinometers, piezometers, extensometers, etc.) are available in the landslide area, development of other applications of the FLAIR model is possible since the mobility function $Y(\cdot)$ can be correlated to field data concerning the movement of landslides or changes in pore pressure. A study has been developed for modeling the movement of a landslide located near the town of Assisi (Central Italy) on the northwestern flank of Mt. Subasio (Graziani et al. 2009). Sliding involves a large wedge in the upper part of an abandoned quarry where well-stratified limestones of the Maiolica formation, rich in clay-marly interbeds, had been mined. A very large potential slide involving a 140,000 m³ wedge was first detected in 2003. This movement date was adopted to calibrate the model and then to identify the mobility function. Geotechnical investigations were carried out, and displacements of the slope were monitored by surface measurements and probe inclinometers. The rainfall regime was linked to surface monitoring comprising two continuous-reading wire extensometers measuring tension crack widening and measurement of displacements of the quarry faces by conventional surveying techniques.

The analyzed measurements covered a period of 18 months (March 2005 to August 2006). During this time, a failure occurred in December 2005 (600 m³ in volume) after prolonged rainfall. The extensometer data were elaborated to allow a useful comparison to be made with the mobility function and to verify the FLAIR model results. The graph in Fig. 6 shows this elaboration, comparing the average pattern recorded by the extensometers with the trend of the mobility function $Y(\cdot)$ and demonstrating good agreement between them. Function $Y(\cdot)$ shows, in fact, the same trend of the displacement function. In particular, it was able to simulate, with temporal correspondence, the evolution of the maximum displacements (highlighted with a rectangle in the figure). Moreover, increases and decreases in the mobility function corresponded to displacement behavior of the landslide body. A similar application is discussed in Capparelli et al. (2009a,b) for a case study located in Calabria region (Southern Italy) for a landslide instrumented with inclinometers.

The physically based model SUSHI

General description

SUSHI model describes subsoil water circulation in a bidimensional domain ($\Omega \subset \mathcal{R} \times \mathcal{R}$) which can be defined by irregular soil stratigraphy and different hydrogeological characteristics. It comprises two modules: a hydrological-hydraulic module (Hydro_SUSHI) for studying subsoil water circulation, with particular emphasis on filtration phenomena and spatial-temporal changes in porewater pressure and a geotechnical module (Geo_SUSHI) for evaluating slope stability (Capparelli 2006). The Hydro_SUSHI module is based on the Richards equation, expressed as a function of the suction (ψ). In a Cartesian orthogonal system Oxz , with the z -axis positive downwards, the relevant equation is:

$$\frac{\partial}{\partial x} \left[K(\psi) \frac{\partial \psi}{\partial x} \right] + \frac{\partial}{\partial z} \left[K(\psi) \left(\frac{\partial \psi}{\partial z} - 1 \right) \right] = C_{SU}(\psi) \frac{\partial \psi}{\partial t} \quad (15)$$

where $K(\psi)$ is the hydraulic conductivity dependent on suction ψ for non-saturated terrain. In Eq. 15, the relation $K_x(\psi) = K_z(\psi) = K(\psi)$ follows from the assumption that the soil is isotropic. The coefficient $C_{SU}(\psi)$ has been introduced for simulating water flow both in unsaturated and saturated zones. After Paniconi et al. (1991), the coefficient $C_{SU}(\psi)$ models the specific capillary capacity $C(\psi)$ for unsaturated conditions and the storage coefficient $S_s = m_v \gamma_w$ for saturated conditions (m_v is the coefficient of volume compressibility and γ_w is the unit weight of water).

The coefficient is expressed as:

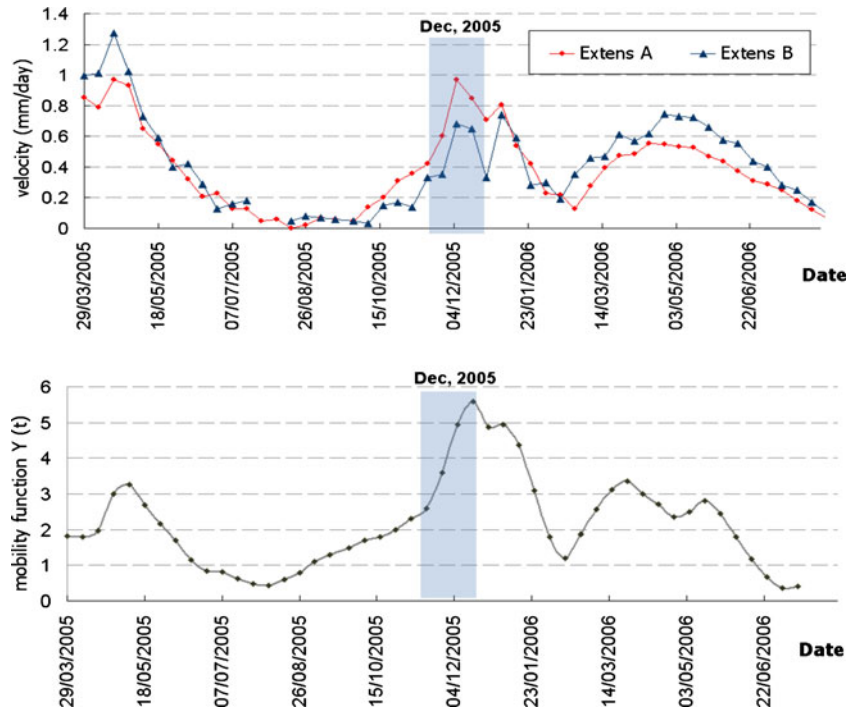
$$C_{SU}(\psi) = \frac{\theta}{n} S_s + C(\psi) \quad (16)$$

where θ is the volumetric moisture content and n is the porosity of the soil. $C(\psi)$ represents the rate at which a soil absorbs or releases water when there is a change in pressure head, equal to the slope of an experimentally determined soil-water characteristic curve, relating volumetric water content to pressure head. When $\psi \geq 0$ (saturated zone), changes in soil volume are mainly related to the compressibility of the soil skeleton; when $\psi < 0$ (unsaturated zone), volume changes are primarily related to changes in moisture content.

The Richards equation does not allow analytical solutions except in cases where simplifying hypotheses and/or particular boundary conditions are introduced (Basha 1999; Iverson 2000; Chen et al. 2003). There are several two- or three-dimensional case studies of the infiltration phenomenon, performed using less restrictive hypotheses regarding the hydraulic and physical characteristics of the soils, for which numerical solutions are proposed (Hogart and Parlange 2000; Weeks et al. 2004; Menziani et al. 2007). In the SUSHI model, the finite difference method and fully implicit method (Wang and Anderson 1995) are adopted for mathematical solution. Therefore, Eq. 15 takes the following form:

$$\begin{aligned} & \frac{1}{\Delta x} \left[K(\psi_{i+1/2,j}) \left(\frac{\psi_{i+1,j} - \psi_{i,j}}{\Delta x} \right) - K(\psi_{i-1/2,j}) \left(\frac{\psi_{i+1,j} - \psi_{i,j}}{\Delta x} \right) \right] \\ & + \frac{1}{\Delta z} \left[K(\psi_{i,j+1/2}) \left(\frac{\psi_{i,j+1} - \psi_{i,j}}{\Delta z} - 1 \right) - K(\psi_{i,j-1/2}) \left(\frac{\psi_{i,j} - \psi_{i,j-1}}{\Delta z} - 1 \right) \right] \\ & = C_{SU}(\psi_{i,j}) \left(\frac{\psi_{i,j}^{(k+1)} - \psi_{i,j}^{(k)}}{\Delta t} \right) \end{aligned} \quad (17)$$

Fig. 6 Comparison of measured displacements with simulated mobility function



where Δx , Δz is the grid size; $i \pm 1/2, j$ and $i, j \pm 1/2$ indicate quantities evaluated at the spatial coordinates $(x_0 + (i \pm 1/2)\Delta x, z_0 + j\Delta z)$ and $(x_0 + i\Delta x, z_0 + (j \pm 1/2)\Delta z)$; Δt is the time step; and (k) and $(k+1)$ are the time-step indices evaluated at times $t = t_0 + k\Delta t$ and $t = t_0 + (k + 1)\Delta t$.

Validation tests have been carried out (Capparelli 2006) to compare model outputs with numerical or experimental solutions proposed in the literature (Vauclin et al. 1979; Paniconi and Putti 1994), reproducing accurately the flow fields, the hydraulic characteristics of the soil, and the boundary and initial conditions considered by the authors. The comparison of results was found to be satisfactory and has confirmed the capability of the model to simulate groundwater circulation.

Hydro_SUSHI takes into account the evapotranspiration process, whose contribution can strongly influence the water balance of the unsaturated zone. The water losses in the unsaturated zone may in fact have a significant influence on groundwater recharge and the resulting levels and consequently on the stability of a slope (Van Asch et al. 2009). This is particularly true when the shallow layers play a central role in slope stability and long periods are simulated, including the summer seasons.

Water loss is related to the separate phenomena of crop transpiration and soil evaporation when simulating subsurface water flow. Following a broad approach, water loss is specified by potential evapotranspiration, for which there is an upper limit to evapotranspirative demand, and subsequently by using soil and canopy characteristics to estimate the actual transpiration (T) and actual soil evaporation (E_s). The term T represents the water uptake by plant roots and can be introduced as a sink term $S [t^{-1}]$ which is added into the Richards equation (e.g., van Dam and Feddes 2000). The maximum possible root water extraction rate integrated over the rooting depth $z_r[L]$ is equal to the potential transpiration rate, $T_p[Lt^{-1}]$, which is mostly governed by atmospheric conditions. In the Hydro_SUSHI model, S is determined in order to account for the

restriction to potential transpiration caused by soil moisture limitations in the case of uniform root distribution, as:

$$S(\psi) = \alpha(\psi) \frac{T_p}{|z_r|} \quad (18)$$

where $\alpha(\psi) \in [0,1]$ is a dimensionless reduction factor depending on the suction ψ (Feddes et al. 1978; Droogers 2000). Integration of $S(\psi)$ according to Eq. 18 over the rooting depth yields the total actual transpiration T . The actual soil evaporation rate E_s is estimated by the Richards equation, using potential evaporation E_{sp} as the upper boundary condition. For each time step, the actual evaporation flux is limited to the maximum possible rate of supply of water to the soil surface in accordance with the Darcy equation. This procedure permits either the application of different methods to estimate the potential evapotranspiration, or the direct use of measured values of E_s and T if these are available.

The Geo_SUSHI module is based on well-known General Limit Equilibrium methods and uses the Fredlund and Rahardjo (1993) slope failure equation for unsaturated soils:

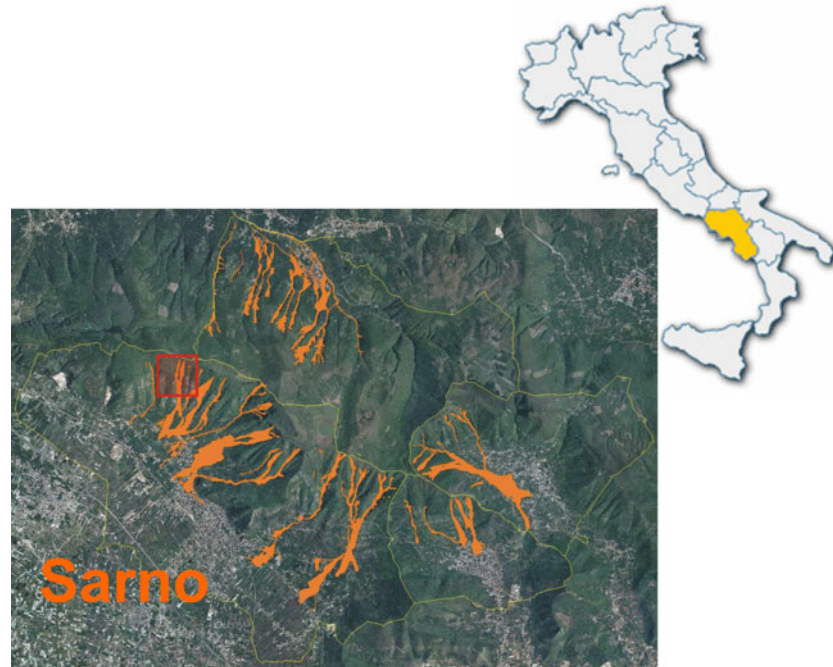
$$\tau = c' + (\sigma - u_a) \tan \phi' + (u_a - u_w) \tan \phi_b \quad (19)$$

where τ is shear strength; c' is effective cohesion; σ is total normal stress; u_a is pore air pressure due to surface tension; u_w is porewater pressure; ϕ' is the effective friction angle; and ϕ_b is the angle expressing the rate of strength increase related to matric suction. In practical applications, ϕ_b has been evaluated by the expression proposed by Vanapalli et al. (1996), which suggests:

$$\tan \phi_b = \left\{ \tan \phi' \left[\frac{\theta(\psi) - \theta_r}{\theta_s - \theta_r} \right] \right\} \quad (20)$$

where θ_r and θ_s are the saturated and residual soil moisture, respectively, and $\theta(\psi)$ is the water content indicated by the retention curve for the suction level ψ .

Fig. 7 Overview of Pizzo d'Alvano massif. Analyzed area shown by the red square



Application to case study

The SUSHI model was applied to an area located in Sarno, in the upper Tuostolo basin, near the slope where mudflows occurred on 5 May 1998 (Fig. 7). Following heavy and prolonged rainfall, many slides developed into mud flows which struck the urban areas of four small towns at the toe of the Pizzo d'Alvano massif: Sarno, Siano, Quindici, and Bracigliano (Campania region, Southern Italy). It was one of the most serious events of its kind in Italy,

and it caused the process of planning risk mitigation measures and civil protection activities to be extensively modified (Versace et al. 2007).

The areas where the landslides took place are mantled by very loose pyroclastic soils which were produced by the explosive phases of Somma-Vesuvius volcanic activity, both as primary air-fall deposits and reworked deposits (paleosols). Air-fall deposits cover a wide area, having been distributed by prevailing winds as

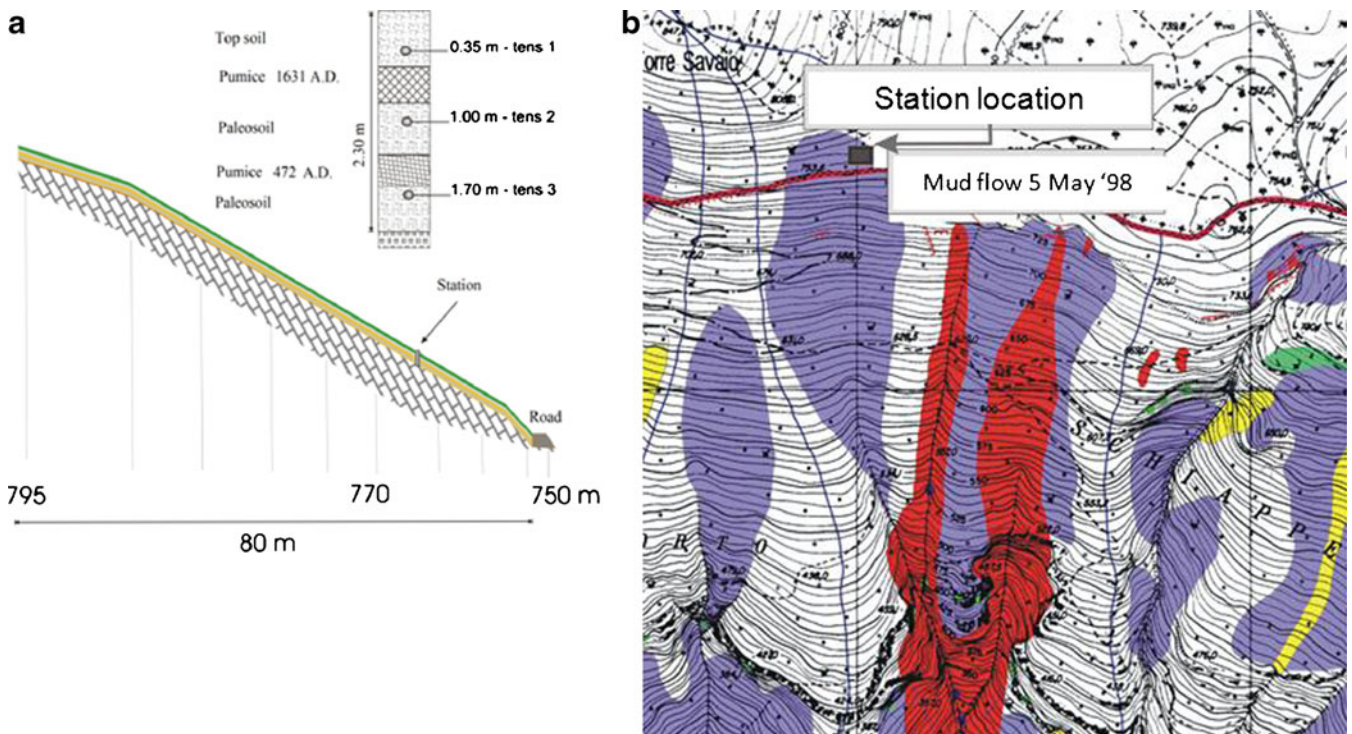


Fig. 8 a Section sketch, geometric and stratigraphic characterization, tensiometer locations. b Overview of the investigated area

Table 1 Hydraulic properties of the involved soil

Layers	θ_s	θ_r	K_s [m/s]
Top soil	0.55	0.14	3.21E-05
Pumice 1631 A.D.	0.82	0.23	3.30E-04
Paleosoil	0.61	0.18	4.00E-06
Pomice 472 A.D	0.68	0.05	1.60E-04

far as 50 km distant. Pumiceous and ashy deposits belonging to at least five different eruptions have been recognized. These materials have a relatively high hydraulic conductivity, and generally, they are not saturated. The total thickness of the pyroclastic covers in these areas varies from a few decimeters up to 10 m near the uppermost flat areas. The general structure of the soil progressively adapts itself to the morphology of the calcareous substratum.

In the Tuostolo basin, a measurement station was established above a road. The station was equipped with “jet fill”-type tensiometers and real-time data acquisition and transmission systems. Records at the station showed that suction generally fluctuates between values close to zero in the wet season and several tens of kPa in the dry season. In order to apply the SUSHI model, on-site surveys determined the stratigraphy, topographic profile, and strata sequence. Laboratory tests were also carried out to define the hydraulic and geotechnical characteristics of the soil. Below the active topsoil layer, the cover comprises a sequence of paleosols and pumice layers from the Somma-Vesuvius eruptions. The tensiometers are positioned at depths of 0.35 m in the topsoil and at 1.00 and 1.70 m in the two paleosols (Fig. 8).

These transmitted suction values every 10 min. For the hydraulic properties of the unsaturated conditions, the best fit of the laboratory data was established using the equation proposed by Van Genuchten and Nielsen (1985). The values of the bubbling pressure, or air entry value, ψ^b , were determined

by the graphical method proposed by Fredlund and Xing (1994). Table 1 shows the values of the main hydraulic characteristics used for the simulation: the saturated moisture content and residual moisture content (θ_s ; θ_r) and the saturated hydraulic conductivity (K_s).

The vegetation over most of the study area is degraded chestnut and oak coppice. Climate data were obtained from a meteorological station located close to the study site. Available data were the minimum and maximum air temperature at a daily time step, from April 2006 to April 2007. In this application, an indirect approach was used to estimate the potential evapotranspiration rate ET_p required by the SUSHI model, by determining it from available weather data using the well-known and low data-intensive Priestley–Taylor equation (Priestley and Taylor 1972), essentially a shortened version of the original Penman combination equation (1948) where the aerodynamic component is reduced to a coefficient α' :

$$ET_p = \alpha' \left[\frac{1}{\lambda} \frac{\Delta}{\Delta + \gamma} (R_n - G) \right] \quad (21)$$

where ET_p is the potential evapotranspiration (mm day^{-1}); α' is assumed to be 1.26 as suggested by the authors and by Lhomme (1996); λ is the latent heat of vaporization (MJ kg^{-1}); Δ is the slope of the saturation vapour pressure–temperature curve ($\text{kPa } ^\circ\text{C}^{-1}$); γ is the psychrometric constant ($\text{kPa } ^\circ\text{C}^{-1}$); R_n is the net radiation ($\text{MJ m}^{-2} \text{day}^{-1}$); and G is the soil heat flux

Fig. 9 Daily values of mean air temperature and potential evapotranspiration ET_p

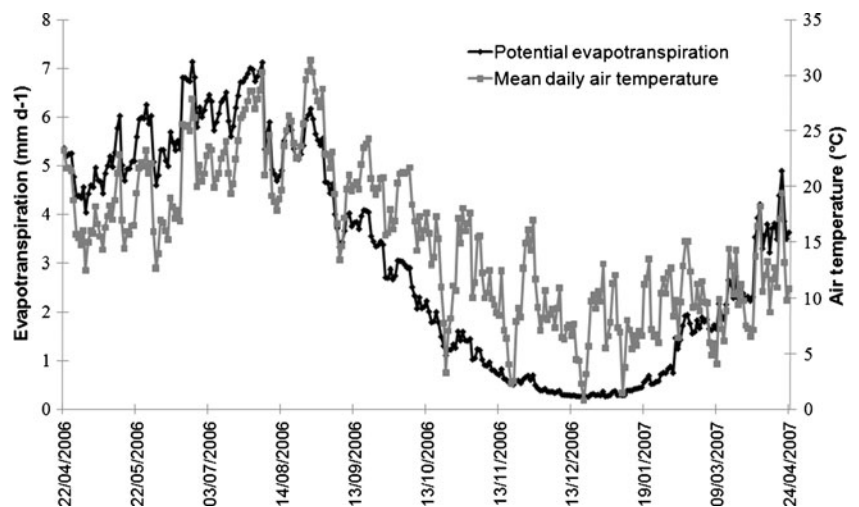
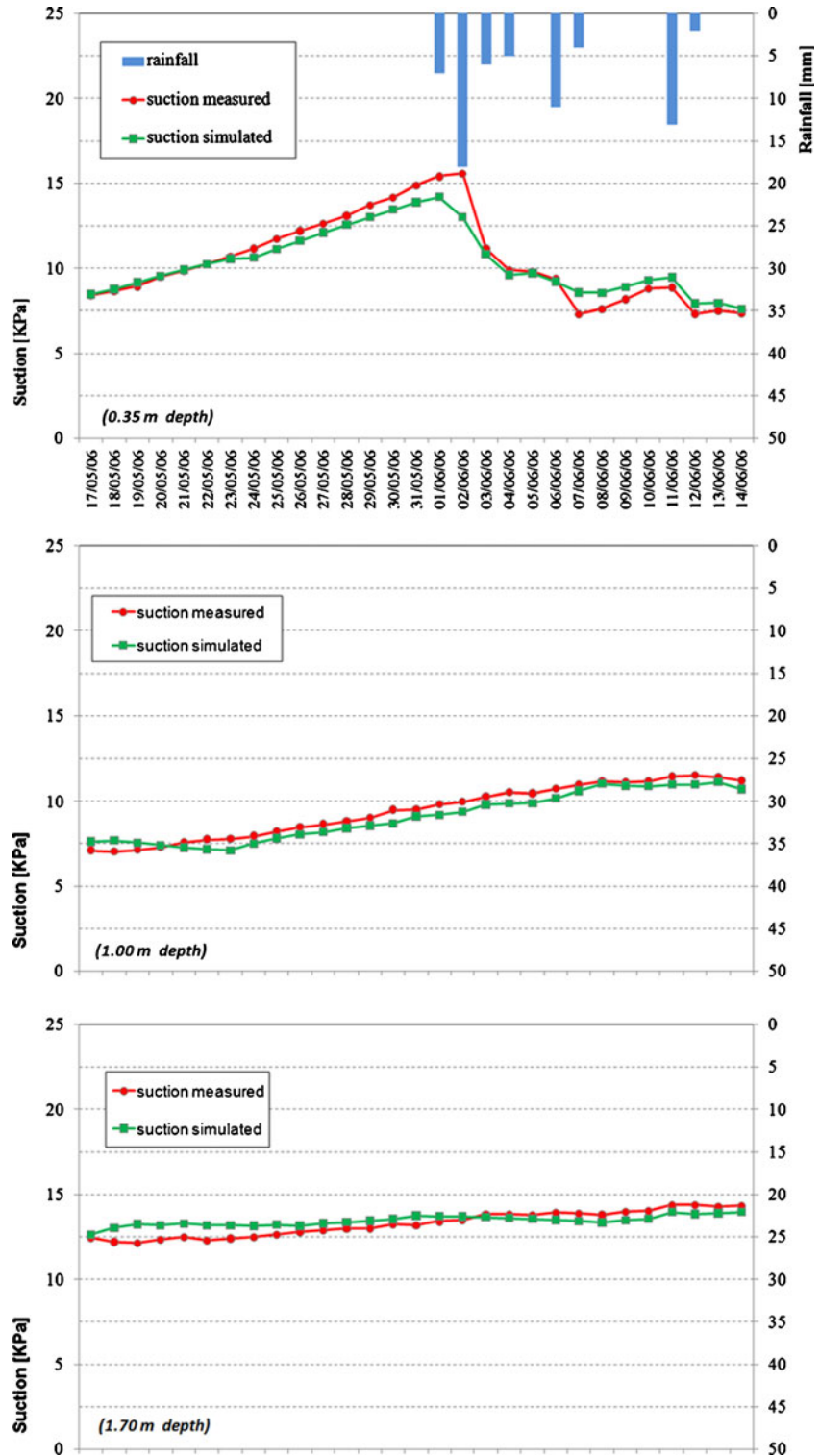


Fig. 10 Comparison between simulated and measured suction data. (Run 1)

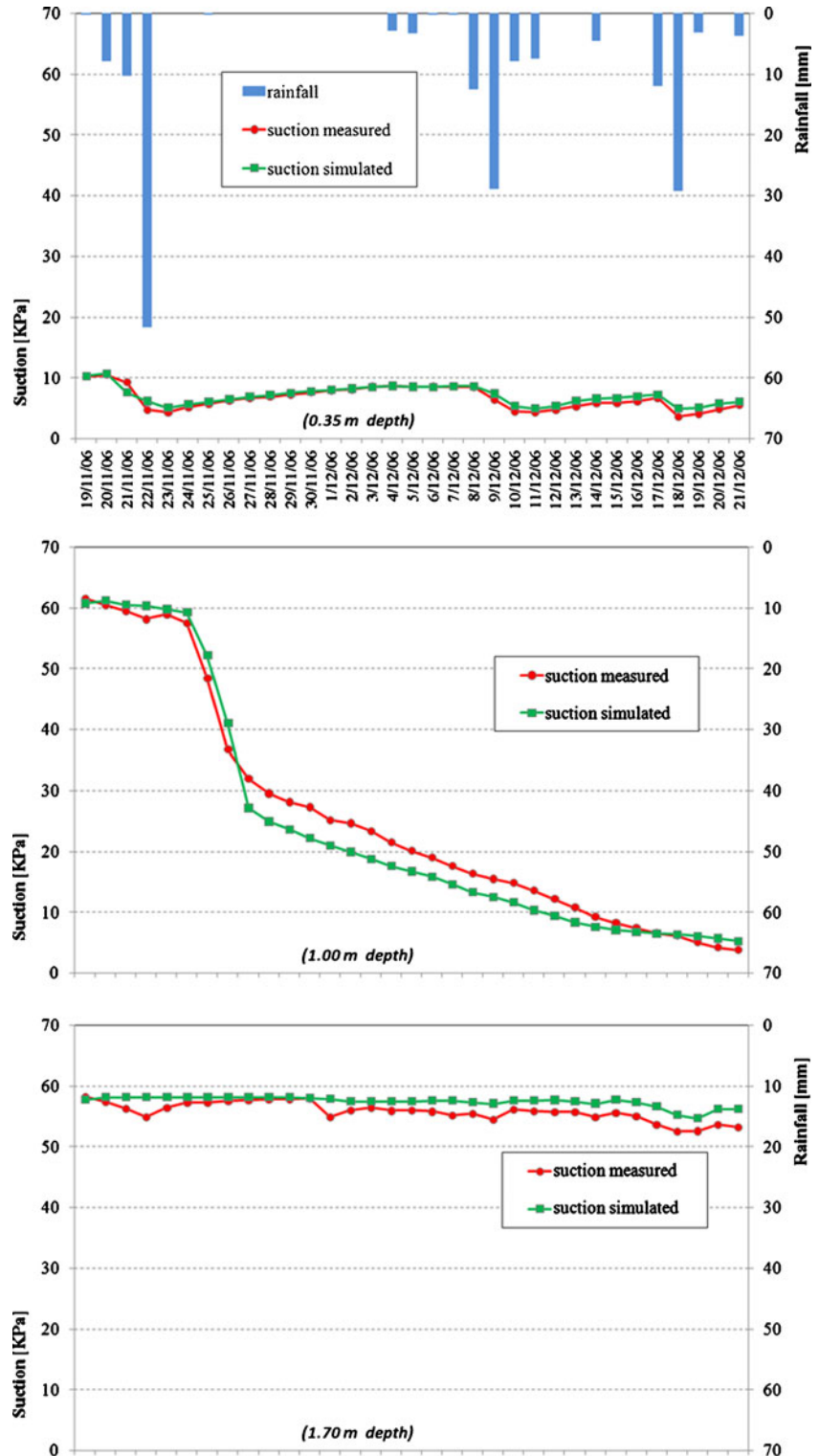


(MJ m⁻² day⁻¹). On a daily scale, G is essentially zero and it can be ignored, while R_n was estimated as the difference between the incoming net shortwave radiation and the outgoing net longwave radiation as recommended in Allen et al. (1998). The other physical variables appearing in Eq. 21, namely the latent heat of vaporization, the slope of the saturation vapour pressure-temperature curve, and the psychrometric constant, have been computed following classical formulations (e.g., Shuttleworth

1993). The potential evapotranspiration gives valid values for well-watered grass and the use of a crop coefficient as advised by the UN Food and Agriculture Organization for other types of crop.

Crop coefficients were not used in this application. Results obtained for the simulation period, together with the observed mean daily air temperatures, are shown in Fig. 9.

Fig. 11 Comparison between simulated and measured suction data. (Run 2)



Diurnal variation of evapotranspiration at the time steps required by the SUSHI model was obtained by distributing the daily values according to a sinusoidal variation over the hours of potential sunlight each day. This method has the advantage that it does not require any meteorological data, but clearly, it cannot take account of the effects on potential evapotranspiration estimates of changing temperatures, humidity, or

cloud cover from hour to hour. Consequently, the potential evaporation E_{sp} for a wet, bare soil, and potential transpiration T_p were evaluated as:

$$E_{sp} = ET_p \exp(-aLAI) \quad (22)$$

$$T_p = ET_p - E_{sp} \quad (23)$$

where α is a parameter accounting for the interception by vegetation of incident solar radiation. As proposed by Huygen et al. (1997), its value was assumed to be 0.5, a value that is valid for most agricultural canopies. *LAI* is the canopy leaf area index ($\text{m}^2 \text{m}^{-2}$). In the absence of more detailed data, *LAI* was assumed to be constant and was set to be equal to 5 (Allen et al. 1998). As suggested in Allen et al. (1998), when z_r in Eq. 18 was unknown, a value of 0.15 m was adopted. The periods which were further examined were:

- 17 May 2006–14 June 2006 (Run 1)
- 19 November 2006–21 December 2006 (Run 2)

representing the dry season and wet season, respectively. The initial conditions were gathered from the tensiometer data on the day before the simulation period, taking particular note of the average value over the 24 h for each depth (0.35, 1.00, and 1.70 m) and assuming linear behavior between two contiguous measurements. These suction distributions were imposed as the initial homogeneous conditions for the whole domain.

Variable boundary conditions, i.e., Dirichlet or Neumann conditions, were imposed on the basis of on-site observations. In particular, no downward flux was permitted at the bedrock where there is a layer of red-dark clayey ashy soil (“regolite”) with rare limestone fragments having a saturated hydraulic conductivity (10^{-8} m s^{-1}) which can be considered very low compared with the overlying layer; similarly, no flux was permitted for the upslope boundary, since field surveys indicated coincidence between the surface and subsurface watershed, making it reasonable to hypothesize that there is no contribution of flow from upstream; for downslope boundary, given that a rocky cliff interrupts the morphological continuity of the slope, mixed boundary conditions were adopted, providing Dirichlet or Neumann conditions on the basis of the saturation degree of the layers; and finally, the boundary conditions at the upper side of domain were managed by the rainfall infiltration.

Application of the model provided a reconstruction of suction behavior over time for each node of the mesh. For all simulations, the suction values were taken to be the daily averages at the nodes that corresponded to the positions of the tensiometers. These were compared with the measured average daily suction. Figures 10 and 11 show a comparison between the simulated and measured suction values for Runs 1 and 2, respectively, for each of the three depths of measurement.

The graphs show significant agreement between the measured and the simulated values, confirming the model’s ability to reproduce the soil water circulation in the subsoil and also its variability in the upper and lower zones. In particular, it is interesting to highlight the model’s ability to simulate the rapid change of suction values at a depth of 1.00 m in Run 2, between 24 and 27 November 2006. The safety factors obtained by the Geo_SUSHI module for both runs were all >1.3 , indicating stable slope conditions.

Conclusions

The main conclusions are summarized as follows:

The FLAIR model acts as a general framework for empirical modeling of rainfall–landslide relationships. Most empirical approaches such as I–D or those based on long-period antecedent

rainfall can be considered to be special cases of the FLAIR structure. Moreover, when using FLAIR, the real rainfall pattern is used rather than mean values, and the flexibility of the transfer function allows a correspondingly flexible set of relationships to be developed. FLAIR can be used for real-time forecasting to also predict future landside hazard conditions by coupling it with a rainfall stochastic generator. The mobility function $Y(\cdot)$ can also be correlated to field data concerning movement of landslide masses or changes in soil porewater pressure.

The SUSHI model is a complete local model combining two modules: one is a hydrological–hydraulic module for studying subsoil water circulation (Hydro_SUSHI) and the other is a geotechnical module for evaluating slope stability (Geo_SUSHI). The hydrological module analyses subsoil water movement in a two-dimensional spatial domain defined by irregular soil stratigraphy having different hydrogeological characteristics. It is based on the Richards equation, expressed as a function of suction. The model is capable of estimating the actual transpiration and actual evaporation and, consequently, their effects on suction levels which predominate in the summer season. Results from the application of the SUSHI model to an instrumented slope in the Sarno Mountains show that it has the capacity to reproduce the suction pattern in the soil during both the wet and dry seasons.

References

- Allen RG, Pereira LS, Raes D, Smith M (1998) Crop evapotranspiration—guidelines for computing crop water requirements: FAO Irrigation and Drainage Paper 56. FAO, Rome
- Basha HA (1999) One-dimensional nonlinear steady infiltration. *Water Resour Res* 35 (6):1697–1704
- Baum RL, Godt JW, Harp EL, McKenna JP, McMullen SR (2005) Early warning of landslides for rail traffic between Seattle and Everett, Washington, U.S.A. In: *Proceedings International of Conference on Landslide Risk Management, Vancouver*, pp 731–740.
- Caine N (1980) The rainfall intensity-duration control of shallow landslides and debris flows. *Geogr Ann* 62A(1–2):23–27
- Campbell RH (1975) Soil slips, debris flows and rainstorms in the Santa Monica mountains and vicinity, Southern California. U.S. Geological Survey Professional Paper 851.
- Cannon SH, Ellen SD (1985) Rainfall conditions for abundant debris avalanches, San Francisco Bay region, California. *Cal Geol* 38(12):267–272
- Capparelli G (2006) Il ruolo della circolazione idrica sotterranea nei pendii soggetti a fenomeni di in stabilizzazione. Dissertation, University of Calabria.
- Capparelli G, Tiranti D (2010) Application of the MoniFLAIR as an early warning system for rainfall-induced landslides in Piedmont region (Italy). *Landslides*. Springer Berlin/Heidelberg doi:10.1007/s10346-009-0189-9
- Capparelli G, Biondi D, De Luca DL, Versace P (2009) Hydrological and complete models for forecasting landslides triggered by rainfalls. In: *Proceedings of the First Italian Workshop on Landslides, 8–10 June 2009, Napoli (Italy)*, pp 162–173.
- Capparelli G, Giorgio M, Greco R, Versace P (2009) Rainfall height stochastic modeling as a support tool for floods and flowslides early warning. In: *Proceedings of 33rd International Association of Hydraulic Engineering & Research (IAHR), Vancouver-British Columbia, 9–14 August 2009*, pp. 6812–6819.
- Cascini L, Versace P (1988) Relationship between rainfall and landslide in a gneissic cover. In: *Proceedings of the fifth International Symposium on Landslides, Lausanne*, pp 565–570.
- Chen JM, Tan YC, Chen CH (2003) Analytical solutions of one-dimensional infiltration before and after ponding. *Hydrol Process* 17:815–822
- Cole K, Davis GM (2002) Landslide warning and emergency planning systems in West Dorset, England. In: McInnes RG, Jakeways J (eds) *Instability, Planning and Management*. Thomas Telford, London, pp 463–470
- Corominas J, Moya J (1999) Reconstructing recent landslide activity in relation to rainfall in the Llobregat River Basin, Eastern Pyrenees, Spain. *Geomorphol* 30:79–93

- D'Orsi RN, D'Avila C, Ortigao JAR, Moraes L, Santos MD (1997) Rio-The Rio de Janeiro landslide watch. In: Proceedings of 2nd PSL Pan-Am Symposium on Landslides, Rio de Janeiro, Vol 1:21–30.
- Droogers P (2000) Estimating actual evapotranspiration using a detailed agro-hydrological model. *J Hydrol* 229:50–58
- Fathani TF, Karnawati D, Sassa K, Fukuoka H, Honda K (2009) Development of landslide monitoring and early warning system in Indonesia. In: Proceedings of The First World Landslide Forum, 18-21 November 2008, Tokyo, pp 195–198.
- Feddes RA, Kowalik PJ, Zaradny H (1978) Simulation of field water use and crop yield simulation monograph series. Wageningen, PUDOC
- Fredlund DG, Rahardjo H (1993) Soil mechanics for unsaturated soils. John Wiley and Sons, INC, New York
- Fredlund DG, Xing A (1994) Equations for the soil-water characteristic curve. *Can Geotech J* 31:521–532
- Gabet EJ, Burbank DW, Putkonen JK, Pratt-Sitaula BA, Ojha T (2004) Rainfall thresholds for landsliding in the Hymalayas of Nepal. *Geomorphol* 63:131–143
- Giorgio M, Greco R, Capparelli G, Versace P (2009) A new empirical predictor of rainfall-induced landslides mobility function. In: Proceedings of The First Italian Workshop on Landslides, 8-10 June 2009, Napoli (Italy), pp 181–185.
- Glade T, Crozier M, Smith P (2000) Applying probability determination to refine landslide-triggering rainfall thresholds using an empirical "Antecedent Daily Rainfall Model". *Pure Appl Geophys* 157(6–8):1059–1079
- Graziani A, Rotonda T, Tommasi P (2009) Stability and deformation mode of rock slide along interbeds reactivated by rainfall. In: Proceedings of The First Italian Workshop on Landslides, 8-10 June 2009, Napoli (Italy), pp 62–71.
- Guzzetti F, Peruccacci S, Rossi M, Stark CP (2007) Rainfall thresholds for the initiation of landslides in central and southern Europe. *Meteorol and Atmos Phys* 98:239–267
- Heneker TM, Lambert MF, Kuczera G (2001) A point rainfall model for risk-based design. *J Hydrol* 247(1–2):54–71
- Hogart WL, Parlange JY (2000) Application and improvement of a recent approximate analytical solution of Richards' equation. *Water Resour Res* 36:1965–1968
- Huygen J, Van Dam JC, Kroess JG, Wesseling JG (1997) SWAP 2.0: input and output manual. Wageningen Agricultural University, Wageningen, The Netherlands
- IFLDM (2007) Proceedings of the international forum on landslide disaster management, 10-14 December, Hong Kong (eds) Ken Ho and Victor Li.
- Iiritano G, Versace P, Sirangelo B (1998) Real-time estimation of hazard for landslides triggered by rainfall. *Environ Geol* 35(2–3):175–183
- ILF (2008) Proceedings of the first world landslide forum, 18-21 November 2008, Tokyo, pp 726
- Iverson RM (2000) Landslide triggering by rain infiltration. *Water Resour Res* 36:1897–1910
- IWL (2009) Proceedings of the first Italian workshop on landslides, 8-10 June 2009, Napoli (Italy) pp 250
- Kalsnes B, Nadim F, Glade T (2009) Study effects of global change on landslide risk. In: Proceedings of The First World Landslide Forum, 18-21 November 2008, Tokyo, pp 19–33.
- Keefer DK, Wilson RC, Mark RK, Brabb EE, Brown WM III, Ellen SD, Harp EL, Wieczorek GF, Alger CS, Zatkun RS (1987) Real-time landslide warning during heavy rainfall. *Science* 238:921–926
- Lhomme J-P (1996) A theoretical basis for the Priestley-Taylor coefficient. *Bound-Layer Meteorol* 82:179–191
- Menziani M, Pugnaghi S, Vincenzi S (2007) Analytical solutions of the linearized Richards equation for discrete arbitrary initial and boundary conditions. *J Hydrol* 332:214–225
- Montgomery DR, Dietrich WE (1994) A physically based model topographic control on shallow landsliding. *Water Resour Res* 30:1153–1171
- Paniconi C, Putti M (1994) A comparison of Picard and Newton iteration in the numerical solution of multidimensional variably saturated flow problems. *Water Resour Res* 30(12):3357–3374
- Paniconi C, Alvaro AA, Wood EF (1991) Numerical evaluation of iterative and noniterative methods for the solution of the nonlinear Richards equation. *Water Resour Res* 27(6):1147–1163
- Priestley CHB, Taylor RG (1972) On the assessment of surface heat flux and evaporation using large scale parameters. *Mon Weather Rev* 100:81–92
- Pun WK, Wong ACW, Pang PLR (2003) A review of the relationship between rainfall and landslides in Hong Kong. In: Proceedings of the 14th Southeast Asian Geotechnical Conference. Vol 3:211–216
- Rigon R, Bertoldi G, Over TM (2006) Geotop: a distributed hydrological model with coupled water and energy budgets. *J hydrometeorol* 7(3):371–388
- Shuttleworth WJ (1993) Evaporation. In: Maidment DR (ed) Handbook of hydrology. McGraw-Hill, Inc, p 1424
- Sirangelo B, Versace P (1992) Modelli stocastici di precipitazione e soglie pluviometriche di innesco dei movimenti franosi. In: Proceedings of XXIII Convegno Nazionale di Idraulica e Costruzioni Idrauliche, Florence (Italy), Vol D: 361–373.
- Sirangelo B, Versace P (1996) A real time forecasting for landslides triggered by rainfall. *MECC* 31:1–13
- Sirangelo B, Versace P, Iiritano G (1998) The performances of the FLAIR model in the analysis of different landslides". *Atti del convegno "XXIII EGS General Assembly", Nice (FRA)*, 1998.
- Sirangelo B, Versace P, Capparelli G (2003) Forwarning model for landslides triggered by rainfall based on the analysis of historical data file. In: Servat E, Najem W, Leduc C, Shakeel A (eds), Hydrology of the Mediterranean and Semi-Arid Regions, IAHS Publ. 278 (Red Book), pp. 298–304
- Sirangelo B, Versace P, De Luca DL (2007) Rainfall nowcasting by at site stochastic model P.R.A.I.S.E. *Hydrol Earth Syst Sci* 11:1341–1351
- Takara K, Apip Bagiawan A (2009) Study on early warning system for debris flow and landslide in the Citarum River Basin, Indonesia. In: Proceedings of The First World Landslide Forum, 18-21 November 2008, Tokyo, pp 573–576.
- Tsai TL, Yang JC (2006) Modelling of rainfall triggered shallow landslide. *Environ Geol* 50:525–534
- UNDR0 (1991) Mitigation natural disaster. In: Phenomena, Effects and Options. United Nations, New York, p 164
- van Asch WJ, van Beek LPH, Bogaard TA (2009) The diversity in hydrological triggering systems of landslides. In: Proceedings of The First Italian Workshop on Landslides, 8-10 June 2009, Napoli (Italy), pp 151–156.
- van Dam JC, Feddes RA (2000) Numerical simulation of infiltration, evaporation and shallow groundwater levels with the Richards equation. *J Hydrol* 233:72–85
- van Genuchten M-T, Nielsen DR (1985) On describing and predicting the hydraulic properties of unsaturated soils. *Ann Geophys* 3(5):615–628
- Vanapalli SK, Fredlund DG, Pufahl DE, Clifton AW (1996) Model for the prediction of shear strength with respect to soil suction. *Can Geotech J* 33:379–392
- Vauclin M, Khanji D, Vachaud G (1979) Experimental and numerical study of a transient, two-dimensional unsaturated-saturated water table recharge problem. *Water Resour Res* 15(5):1089–1101
- Versace P, Capparelli G (2008) Empirical hydrological models for early warning of landslides induced by rainfall. In: Proceedings of The First World Landslide Forum, 18-21 November 2008, Tokyo, pp 627–630.
- Versace P, Capparelli G, Picarelli L (2007) Landslide investigations and risk mitigation. The Sarno case. In: Ho K, Li V (ed), Proceedings of 2007 International Forum on Landslide Disaster Management, Vol 1, Hong Kong, pp. 509–533
- Wang HF, Anderson MP (1995) Introduction to groundwater modelling- finite difference and finite element methods. Academic Press, Elsevier Science
- Weeks SW, Sander GC, Braddock RD, Matthews CJ (2004) Saturated and unsaturated water flow in inclined porous media. *Environ Model and Assess* 9:91–102
- Wieczorek GF (1987) Effect of rainfall intensity and duration on debris flows in central Santa Cruz Mountains, California. *Geol Soc of Am, Rev in Eng Geol* 7:93–104
- Wilson RC, Wieczorek GF (1995) Rainfall thresholds for the initiation of debris flow at La Honda, California. *Environ and Eng Geosci* 1(1):11–27
- Yano K, Senoo K (1985) How to set standard rainfalls or debris flow warning and evacuation. Sabo Symposium, SEDD Japan, pp 451–455
- Yu YF, Lam JS, Siu CK, Pun WK (2004) Recent advance in landslide warning system. In: Proceedings of the 1 day Seminar on Recent Advances in Geotechnical Engineering, organized by the Hong Kong Institution of Engineers Geotechnical Division, pp 139–147.

G. Capparelli ✉ · **P. Versace**
 Dipartimento di Difesa del Suolo,
 Università della Calabria,
 Rende, Italy
 e-mail: kgiov@dds.unical.it